Journal of Alloys and Compounds 509 (2011) 7729–7737

Contents lists available at ScienceDirect

Journal of Alloys and Compounds

journal homepage: www.elsevier.com/locate/jallcom

Structural and magnetic properties of nanostructured $Fe_{50}(Co_{50})$–6.5 wt% Si powder prepared by high energy ball milling

M. Khajepour, S. Sharafi*

Materials Science and Engineering Department, Shahid Bahonar University of Kerman, Kerman, Iran

ARTICLE INFO

Article history:
Received 12 October 2010
Received in revised form 14 April 2011
Accepted 16 April 2011
Available online 23 April 2011

Keywords:
Mechanical alloying
Nanostructured materials
Saturation magnetization
Coercivity

ABSTRACT

This work investigates the effects of 6.5 wt% Si addition and milling times on the structural and magnetic properties of $Fe_{50}Co_{50}$ powders. For this purpose, at first the elemental Fe and Co powders were milled for 10 h to produce $Fe_{50}Co_{50}$ alloy and then Si was added and the new product was milled again for different times. The microstructural and magnetic properties were investigated by X-ray diffraction (XRD), scanning electron microscopy (SEM) and vibrating sample magnetometer (VSM). The results show that the minimum crystallite size of the as-milled powders (~12 nm) has been achieved after introducing Si and milled for 8 h (total milling time of 18 h). Also an amount of 188 emu/g has been achieved for M_s. This amount of M_s is higher than most of those which have been already reported for M_s of different Fe–Si systems.

1. Introduction

Magnetic materials have revolutionized our lives. These materials are used in electronic, computer and telecommunication industries. During the last decades different types of magnetic materials have been used including pure iron and its alloys [1]. Pure iron is a good ferromagnetic material; however the resistivity of iron is very low, i.e. it experiences high eddy current losses [2]. When eddy currents are induced in materials two main effects are observed: incomplete magnetization of the materials (skin effect) and increase in core losses [1]. However, alloyed iron provides higher magnetic permeability and lower total core losses and results in devices having higher efficiencies than devices using pure iron cores [2]. On the other side according to their coercivity value, the magnetic materials traditionally classified into three main groups: soft magnetic materials, recording materials and hard magnetic materials [3]. Soft magnetic materials are known by several characteristics such as: high saturation magnetization (M_s), high permeability (μ), small coercive field (H_c), small remanence (M_r), small hysteresis loop, rapid response to high frequency magnetic fields and high electrical resistivity [4].

Among different iron-based nanocrystalline soft ferromagnetic alloys, Fe–Si nanocrystalline soft magnetic powders have a significant potential for applications like electric/magnetic measurements, information storage, transformer magnets and magnetic cores [5–8]. The addition of proper amounts of Si to Fe not only results in decrement of magnetic anisotropy and coercive force but also increment of electrical resistivity and, thereby, reduction of eddy current losses [7,9]. 6.5 wt% Si–Fe is a well known alloy due to its excellent soft magnetic properties such as high saturation magnetization, near zero magnetostriction and high resistivity, which suggests that the core loss should be reduced compared to those of comparable alloys with 3–4 wt% silicon [1,5,10]. Referring to saturation magnetization definition as the number of magnetic moments parallel to the applied field per unit volume of the material, increasing the Si content of alloys unfortunately leads to decrement of Fe content as a ferromagnetic component (since Si is a diamagnetic element) and thereby can reduce the saturation magnetization [7]. Therefore, it will be useful to have a procedure which can prevent this function.

As the Fe–Co soft magnetic alloy has low coercive field, low hysteresis loss, low eddy-current loss, high electric permeability and high saturation magnetization, it has been extensively investigated in the previous works on many aspects such as electronic structures, mechanical properties and structural transformations [11,12]. Iron–cobalt alloys have the highest saturation magnetization of all known magnetic alloys [13]. Although the maximum saturation magnetization (M_s) occurs at a concentration of 35 at.% Co, equiatomic compositions offer a considerably larger permeability for similar M_s [13–15].

Compared to their polycrystalline counterparts, the nanostructured materials have showed superior magnetic properties due to single domain configuration [16]. Magnetic nanocrystalline materials are formed by an assembly of regions of coherent crystalline structure (the grains), having an average dimension of the order of nanometer, exhibiting magnetic order and embedded in a

* Corresponding author. Tel.: +98 341 211 4041; fax: +98 341 211 1865.
E-mail address: sh_sharafi@mail.uk.ac.ir (S. Sharafi).

0925-8388/$ – see front matter © 2011 Elsevier B.V. All rights reserved.
doi:10.1016/j.jallcom.2011.04.095

magnetic or nonmagnetic matrix. The matrix can be corresponded to either the grain boundary regions or a phase having structure and/or composition different from that of the main one and being amorphous or nanocrystalline [3]. These materials are fabricated through various methods including inert gas condensation, electrodeposition, sol–gel process, mechanical alloying (MA), chemical vapor condensation (CVC) and heat treatment of rapidly solidified melts [6,15,16]. Among these, MA is one of the useful methods due to relatively inexpensive equipment and readily to produce nanostructure materials and with this method there is the potential to scale-up production for commercial quantities [17]. Therefore, this method has been widely used to synthesize a variety of non-equilibrium materials such as supersaturated solid solution, metastable crystalline, quasi phases, nanostructure and amorphous materials [2,18,19]. In this study, nanocrystalline Fe_{50}–Co_{50} alloy powders (which has the maximum value of saturation magnetization among the Fe–Co alloys) were prepared by mechanical alloying and then Si was added and the effects of Si addition and milling times on structural and magnetic properties are investigated.

2. Experimental

The starting materials used in this study included high purity Fe, Co and Si powders with particle size of <100, <3 and <10 μm, respectively. Mechanical alloying was started by milling $Fe_{50}Co_{50}$ mixed powder composition up to 10 h. Then in order to investigate the effects of milling times and addition of Si, Si was added to make the alloy with composition of [$Fe_{50}(Co_{50})$]–6.5 wt% Si and was milled for 1, 4, 8, 10, 20, 35 and 45 h. The milling process was performed under argon atmosphere (99.9% purity) by using Fritsch planetary ball mill with 250 ml steel container that was loaded with a blend of steel balls (m_1 = 4 g and m_2 = 30.9 g) and rotated at 400 rpm. The ball to powder weight ratio (BPR) was about 20:1 and milling was carried out using a sequence of 30 min milling and 15 min resting. To determine crystallite size, lattice micro-strain, lattice parameter and phase analysis of powder particles, the powder specimens were analyzed by an X-ray diffractometer (Bruker's D8 system, Germany) using Cu Kα (λ = 0.15405 nm) radiation over 20–140 2θ. The crystallite size and lattice micro-strain were estimated by Williamson–Hall method and to determine full-width at half maximum (FWHM) precisely, both Xfit and Sigmaplot software were used. A scanning electron microscope (Camscan mv2300) was used to investigate the powder morphology and magnetic properties were estimated using a magnetometer VSM.

3. Results and discussion

3.1. Morphology

During mechanical alloying, powder particles are subjected to severe mechanical deformation and are repeatedly deformed, cold welded, fractured and rewelded [19]. Fig. 1 shows the SEM micrographs of powder mixtures for various conditions. The starting powders (Fig. 1a) have both spherical and flake shapes of iron with tiny cobalt particles. After 10 h of milling time, the powders form particles with irregular shape and size (Fig. 1b) due to the success of the cold welding. Fig. 1c illustrates the morphology of pervious product after introducing the Si powders without any further milling. The agglomerated particles can be observed after 1 h additional milling (Fig. 1d) and after 4 h the size of particles is diminished and there is no evidence of agglomerated particles (Fig. 1e). Milling up to 20 h has led to more uniform particle size distribution, but still some large particles can be seen around the small size particles (Fig. 1f). Excess milling (up to 35 h) has produce more uniform size distribution of particles (Fig. 1g) and prolonged milling (up to 45 h) does not remarkably affected the size distribution (Fig. 1h). Comparing Fig. 1g with Fig. 1h indicates that the steady state for size distribution of particles has been achieved after 35 h of milling due to the balance between cold welding and fracturing processes. It is generally known that high-energy ball milling processes reach a steady state in which the particles have a homogeneous size and shape [6].

Fig. 2a depicts the lamellar structure that has been achieved after 10 h milling of Fe_{50}–Co_{50}. This type of structure has been seen after milling of the most metallic systems [2]. After adding Si (Fig. 2b) and additional milling for 1 h (Fig. 2c), the Si particles are fractured (Si is brittle compared with Fe and Co) and small size Si particles have diffused to the lamellar particles and formed agglomerated particles with different sizes and shapes. As shown in Fig. 2d, further milling up to 8 h again has led to lamellar structure. This can be due to the dissolution of Si in the structure, and the second stage of the alloying might be taken place. Prolonged milling has caused the work hardening of particles and fracturing to occur (Fig. 2e). In this stage, cold working has been dominated by fracturing.

3.2. Structural properties

X-ray diffraction pattern of the initial Fe_{50}–Co_{50} powders (Fig. 3) shows the presence of bcc-Fe peaks and those of Co with two structures fcc and hcp. After milling for 10 h (Fig. 4a) the diffusion of Co into the bcc-Fe structure has led to the formation of disordered bcc-$Fe_{50}(Co_{50})$ solid solution [14]. During this interval, as fcc-Co phase is metastable at room temperature, it becomes unstable and transforms to the hcp one [14,20]. With the introduction of Si to bcc-$Fe_{50}(Co_{50})$ solid solution and without any further milling, both characteristic peaks of Si and solid solution is observed (Fig. 2b). By milling the new system (bcc $Fe_{50}(Co_{50})$–6.5 wt% Si) for 4 h, the reflection corresponding to Si has disappeared which might be due to the dissolution of Si in the bcc $Fe_{50}(Co_{50})$ solid solution and a new bcc-Fe(Co,Si) solid solution has been formed.

Fig. 5 shows the 3D X-ray diffraction patterns of powders at different conditions. The peaks of pure Fe (Fig. 3a) have high intensities and their width are narrow, but with introduction of Co and subsequent milling up to 10 h, the intensities of diffraction pattern have diminished and the peaks have become broadened due to the refinement and the existence of heterogeneous strains [21]. On the other hand the milling of bcc $Fe_{50}(Co_{50})$–6.5 wt% Si up to 8 h (total milling time 18 h), causes further decreasing of intensities and broadening of peaks and after that the intensities have increased slightly.

Fig. 6 shows the effect of milling times on crystallite size. The crystallite size and internal micro-strain evolutions for milled powders were carried out by Williamson–Hall method [14]. The crystallite size of pure iron before milling process was about 130 nm, with the addition of Co and milling for 10 h, a rapid decrease of crystallite size (less than 20 nm) is observed. With the introduction of Si and continuing the milling for another 8 h, further refinement occurs slowly to about 12 nm and for extended milling time (45 h), the crystallite size increases to about 16 nm which might be due to the raising powder temperature. The decreasing of crystallite size after milling can be explained by the mechanism proposed by Cantor [22]. Nanocrystallization by ball milling occurs in the following steps. In the early stages of ball milling, work-hardening occurs, the dislocation density increases and a cellular structure develops. In the middle stages of ball milling, a drastic transition from work-hardened to layered nanostructures takes place near the powder surfaces. The layered nanostructure has a well developed granular structure with thickness less than 100 nm and is almost dislocation free. A clear boundary exists between the layered nanostructure and the work hardened regions. It has been suggested that when the dislocation cell size reaches a small critical value as a consequence of the severe and high strain rate deformation, continuous recrystallization takes place and results in the layered nanocrystalline structure. By further milling, the thickness of the layered nanostructure decreases and the layers become subdivided by the rotation of equiaxed region. In the final stages of ball milling, randomly oriented equiaxed regions are produced, containing about 10 nm diameter grains [7,22,23]. The ultimate

crystallite size is reported to be two times larger than the lower equilibrium distance between dislocations, L_c. This distance is given by:

$$\frac{3Gb}{\pi(1-\nu)} \quad (1)$$

where G is the shear modulus, b the Burgers vector, ν the Poisson ratio and h the hardness of the material [24]. It is worthy to note that although the grain sizes have been reduced to a nanometer scale, the size of powder particles are still in the micrometer scale.

The actual lattice parameter was obtained by plotting the calculated lattice parameter for each Bragg's angle (especially at high angles) on the y-axis with the corresponding value of $\cos^2\theta/\sin\theta$ on the x-axis and extrapolating to obtain the intercept on the y-axis. The variation of the lattice parameter is represented in Fig. 7. The lattice parameter reported for the pure bcc-Fe is 0.2866 nm [7]. This parameter for bcc-$Fe_{50}(Co_{50})$ powder mixtures

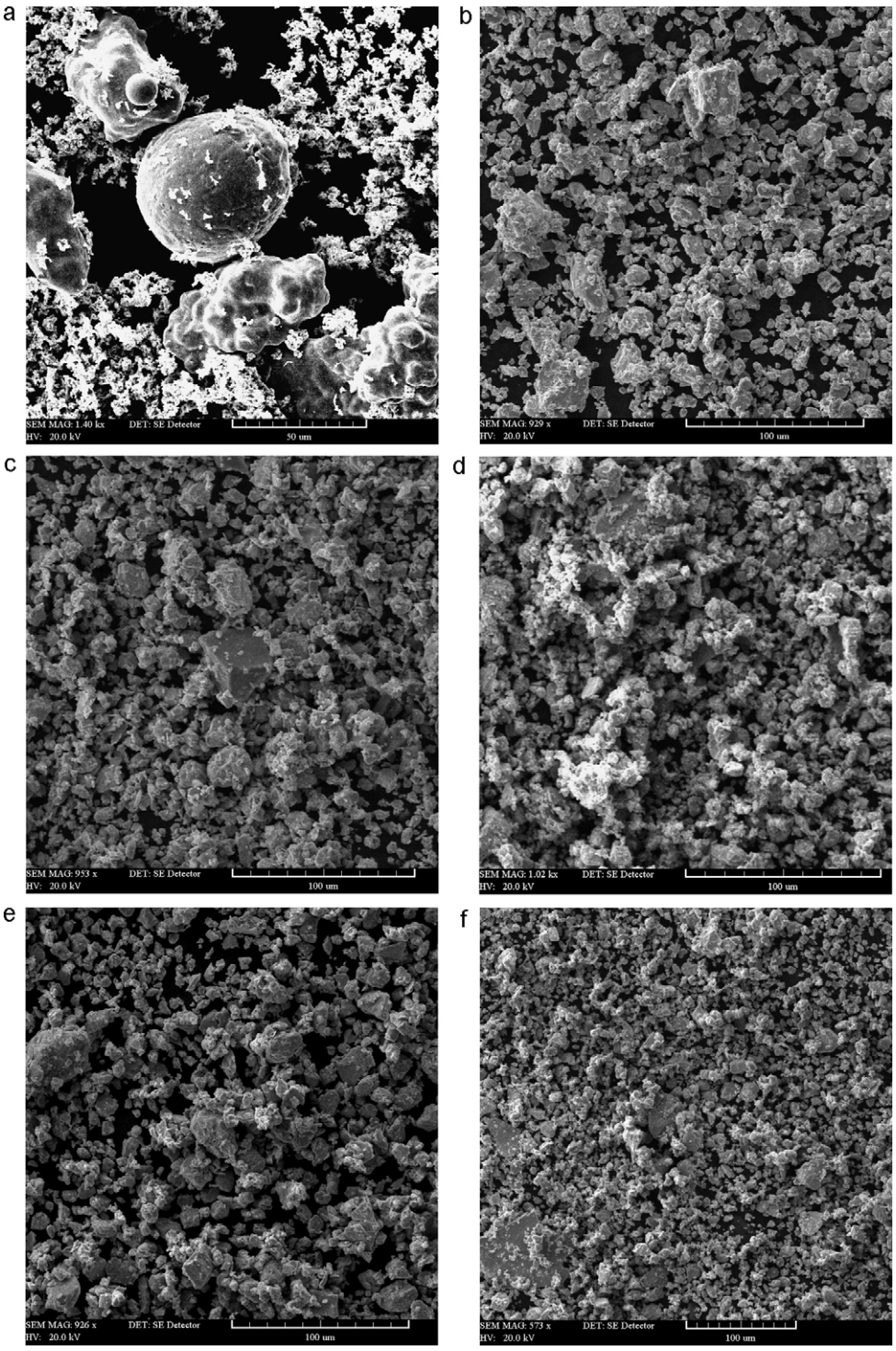

Fig. 1. SEM micrographs for various powders: (a) as-received Fe_{50}–Co_{50} mixture, (b) Fe_{50}–Co_{50} milled for 10 h, (c) Fe_{50}–Co_{50} (10 h milled)–6.5 wt% Si mixture, (d)–(h) Fe_{50}–Co_{50} (10 h milled)–6.5 wt% Si milled for 1, 4, 20, 35 and 45 h, respectively.

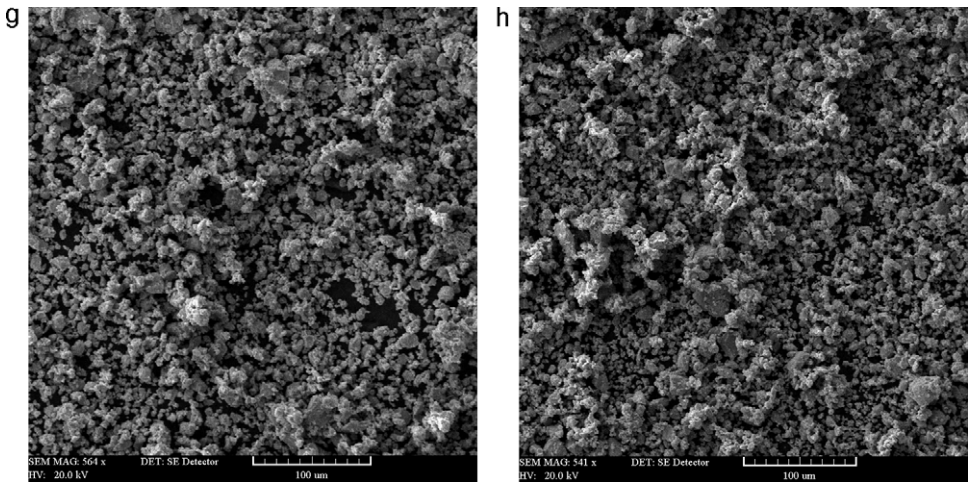

Fig. 1. *Continued*.

diminishes from 0.2866 nm to 0.2862 nm after milling for 10 h due to the alloying of iron with Cobalt and probably to the cobalt allotropic transformation (fcc-hcp) and/or to the triple defect disorder [14]. With progress of the milling process without any Si [14,20], lattice parameter decreases slightly but when Si is added to bcc-$Fe_{50}(Co_{50})$ solid solution and for milled for 8 h, lattice parameter decreases remarkably to a minimum value of 0.2852 nm and after that it increases suddenly for 10 h milling. The increasing evolution of lattice parameter continues for extended milling time. There are two justifications for these variations of lattice parameter after the addition of Si. Firstly since Si has a smaller atomic radius than Fe and Co, dissolution of Si in bcc-$Fe_{50}(Co_{50})$ solid solution causes drastic decreasing of lattice parameter, also milling for longer time (up to 8 h) leads to the dissolution of more Si in the solid solution and probably a supersaturated bcc-Fe(Co,Si) solid solution will be formed. At the same time the crystallite size decreases from 16 nm to a minimum size of 12 nm and production of lattice defects such as dislocations and grain boundaries can increase the energy of the system. Therefore existence of a supersaturated solid solution with high volume fraction of grain boundaries and dislocations and existence of very small grains all together provide a condition in which the Si atoms will be able to leave the grains towards the grain boundaries. This will reduce the energy of the system and therefore the lattice parameter increases. Secondly with decreasing the grain size, the volume fraction of grain boundaries increases. On the basis of the coherent polycrystalline model, the volume fraction of the grain boundaries f_{gb} was estimated by the formula

$$f_{gb} = 1 - f_g \tag{2}$$

where f_g denotes the volume fraction of the grains given by

$$f_g = \frac{(D-d)^3}{D^3} \tag{3}$$

And D is the crystallite size, d is the effective grain-boundary thickness. In most of the nanostructured alloys, the estimated thickness of the interfaces was roughly found at 2–3 atomic layers that is physically consistent with the thickness of the surface layer encountered in non-interacting nanoparticle systems [11]. Consequently, the less dense structure of grain boundaries can result in some negative pressure on the interfaces and this can lead to an increase in the lattice parameter.

Fig. 8 shows the changes of internal micro-strain with milling time. Milling Fe and Co powders up to 10 h (formation of bcc-$Fe_{50}(Co_{50})$ solid solution) will increase the internal micro-strain remarkably. The increase of residual strains inside the material could be due to stress fields associated with the multiplication of the dislocations [7]. Micro-stress in crystallites comes from a number of sources such as vacancies, defects, shear planes, thermal expansions and contractions. Residual stresses in a material produce a distribution of both tensile and compressive forces, which cause peak broadening about the original position in the XRD patterns [2]. After adding Si and doing further milling for additional 1 h, still we observed the increase of strain with time. The micro-strain has continued to increase by increasing milling time and after 8 h of additional milling, the maximum amount of strain is achieved. This behavior is due to the presence of Si, as Si atoms induce more distortion in the lattice. However, further milling up to 10 h leads to decrement of strain. This decrement can be due to diffusion of Si atoms to the grain boundaries and the release of lattice distortion which was induced by the Si solute atoms. After this stage, the strain has increased a small amount. In fact the strain is affected by two different parameters. The first parameter is the migration of Si atoms which decreases the amount of strain and the second one is the severe plastic deformation due to milling process which induces defects. At the end, we observe a small reduction in the amount of strain due to the raising temperature. Generally, the temperature of the powders during milling can be high due to two different reasons. Firstly, it is due to the kinetic energy of the grinding medium. Secondly, it is possible that exothermic processes occurring during the milling process generate heat [21].

3.3. Magnetic properties

In general, some magnetic properties can be improved when the crystallite size is reduced to the nanoscale, while the presence of stresses and defects introduced by mechanical alloying impairs the magnetic property; the overall magnetic property is affected by a competition between decrease in crystallite size and increase in strain [2,14]. Herzer has reported the relationship between magnetic properties and grain size [6] according to random anisotropy model: when the grain size is smaller than the magnetic exchange length the origin of the soft magnetic properties in nanocrystalline materials is ascribed to the averaging out the magneto crystalline anisotropy due to random distribution of the nanoscale grains [25]. The variations of saturation magnetization (M_s) with milling time are shown in Fig. 9. The measured M_s for pure iron is about 186 emu/g, after the addition of Co and milling for 10 h, M_s has increased remarkably and reached to a maximum value of about 225 emu/g. The sharp increment of the M_s suggests that a true alloying process has occurred. The increase of M_s of the

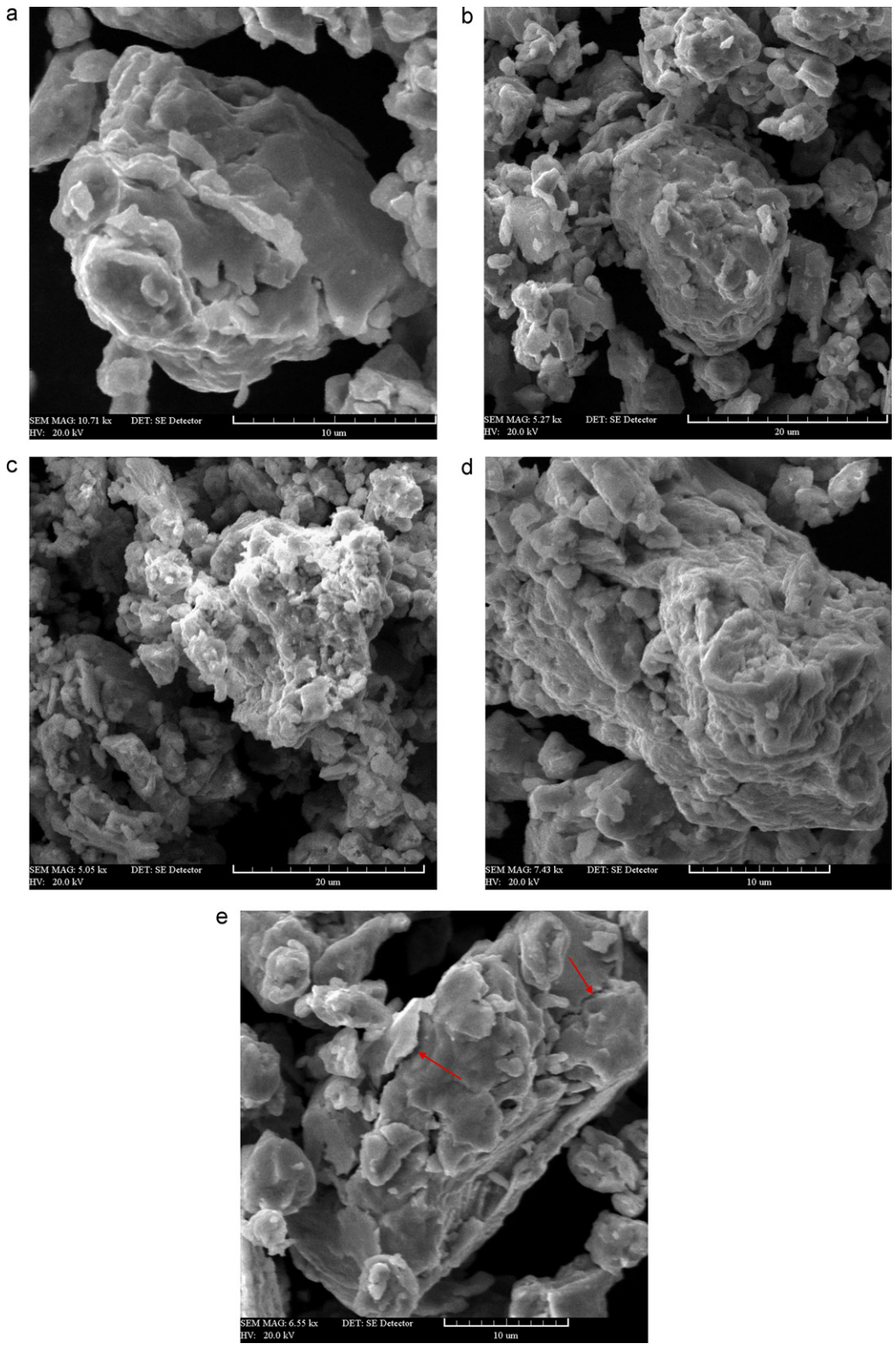

Fig. 2. High magnification SEM micrographs of lamellar structure and agglomerated particles for: (a) Fe_{50}–Co_{50} milled for 10 h, (b)–(d) Fe_{50}–Co_{50} (10 h milled)–6.5 wt% Si milled for 0, 1 and 8 h, respectively, (e) fracturing of large particles to the small ones.

aggregates during milling can be ascribed to the completion of alloying and the diminishing of magnetocrystalline anisotropy due to the grain refinement, which leads to an easier rotation of the magnetic vector. The grain refinement diminishes the magnetocrystalline anisotropy due to averaging the effect of magnetization over randomly oriented nano-sized grains [2,14,19]. Introduction of Si and continuance of milling process lead to the decrement of M_s so that after 8 h milling it reaches to a minimum value and then increases and almost fix at 188 emu/g. The decrease of M_s suggests a remarkable change of magnetic moment during the alloying process due to the modification of the nearest neighbor configuration of the magnetic elements Fe and Co. This is consistent

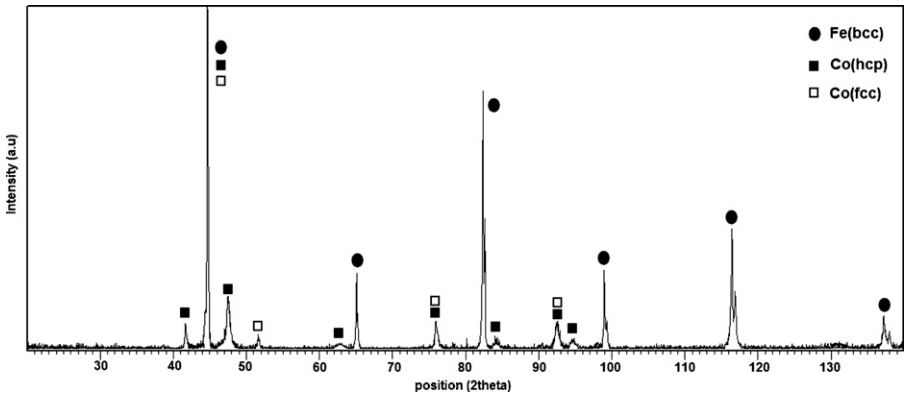

Fig. 3. X-ray diffraction pattern of unmilled Fe_{50}–Co_{50} powder.

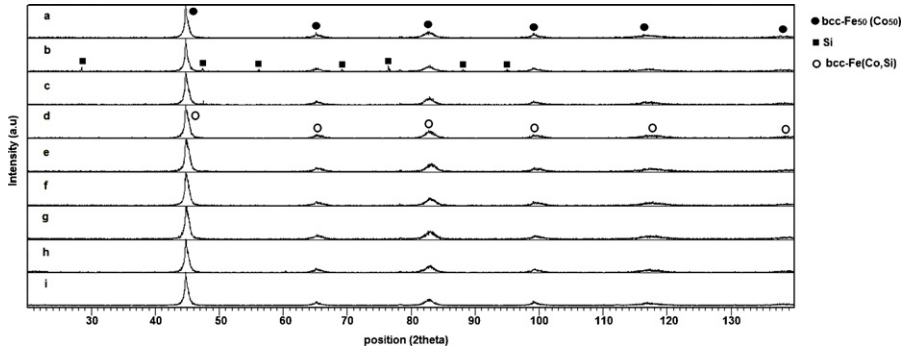

Fig. 4. X-ray diffraction patterns for various conditions: (a) Fe_{50}–Co_{50} (10 h milled), (b)–(i) Fe_{50}–Co_{50} (10 h milled)–6.5 wt% Si milled for 0, 1, 4, 8, 10, 20, 35 and 45 h, respectively.

with the existence of diamagnetic Si atoms in the vicinity of Fe ones which reduced the magnetic moment [26]. Smooth increase of M_s at prolonged milling time may be due to the increase of the lattice parameter [2] and/or completion of alloying process. The saturation magnetization achieved in this work (about 188 emu/g) is reasonable in comparison with the M_s values reported by the other works (between 150 and 175 emu/g) for Fe–Si systems [7,9,26].

Fig. 10 illustrates the variations of coercivity with milling time. Coercivity in general affected by most of defects such as dislocations, grain boundaries and inclusions [13]. The coercivity of crystalline alloys depends strongly on grain size because the magnetic domain walls interact with the grain boundaries. As the grain approaches the exchange length, the averaged magnetocrystalline anisotropy of the random oriented crystallite offers no resistance to the Bloch walls and the coercivity approaches the low values [3]. Fig. 10 shows the addition of Co and milling for 10 h leads to higher coercivity. In the early stages, the grain size exceeds the domain wall thickness and as a result the grain boundaries act as impediments to domain wall motion. Another reason for the increment of the coercivity is the introduction of the microstrain into the material [11,14]. Also the allotropic transformation of Co at this stage can have an influence on coercivity, since hcp structures generally are known to have larger magnetocrystalline anisotropy than fcc ones [26]. By the introduction of Si and continuance of milling process (up to 1 h), the coercivity has increased remarkably. This behavior is due to the increase of internal microstrain which has been introduced during milling, also undissolved Si atoms act as inclusions and hinder the domain walls motion. With extended milling time up to 10 h, the coercivity has decreased. Since dissolution of Si atoms (due to 10 h milling) has diminished the hin-

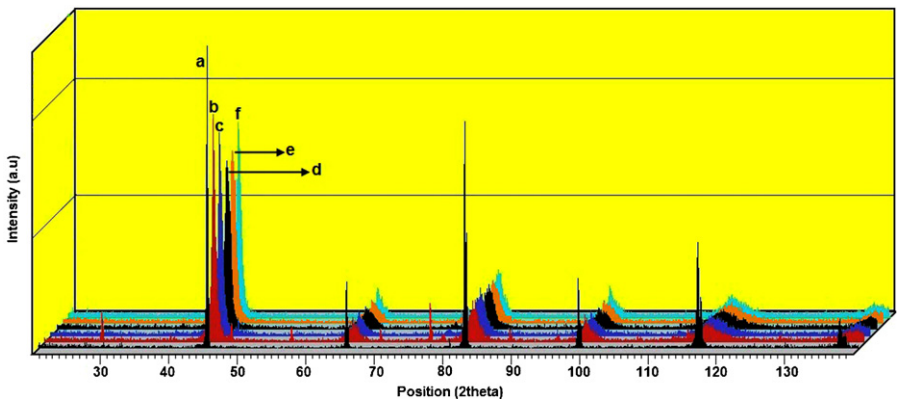

Fig. 5. 3D X-ray diffraction patterns for: (a) pure Fe, (b)–(f) Fe_{50}–Co_{50} (10 h milled)–6.5 wt% Si milled for 0, 1, 8, 10 and 45 h, respectively.

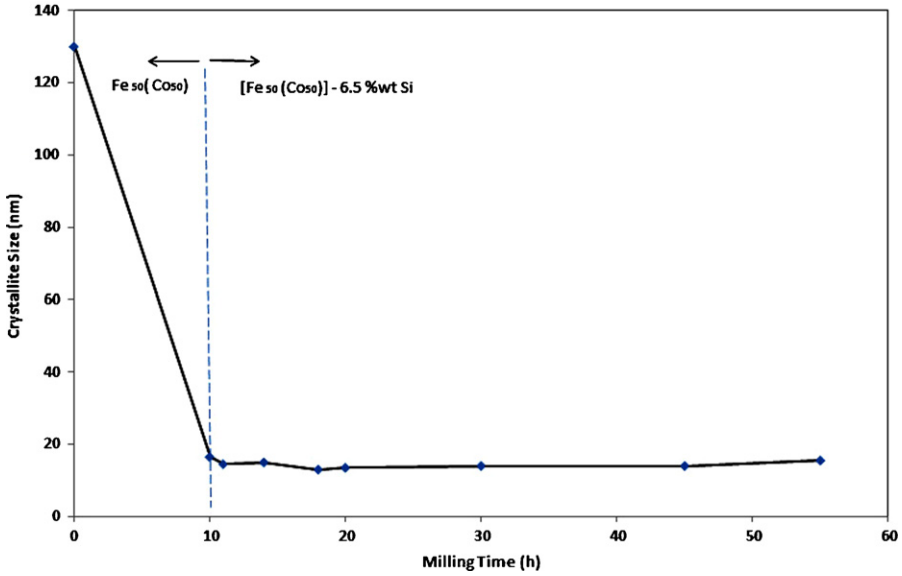

Fig. 6. Variations of crystallite size vs. milling time.

dering of domain walls motion by undissolved Si atoms. Also due to the refinement of crystallites, each grain may act as a single magnetic domain and therefore eliminating the influence of magnetic walls [2]. The increase of coercivity at 8 h may be due to the high values of micro-strain at this stage.

Prolonged milling time leads to the higher amount of coercivity. It was expected that the coercivity decreases at these stages because the grain size is less than the exchange interaction length. When the grain size is larger than the magnetic exchange length, L_{ex}, the coercivity depends on the crystallite size and the saturation magnetization is given by the relation (4):

$$H_c = 3\sqrt{\frac{kT_c k_1}{aM_s}}\frac{1}{D} \tag{4}$$

where D is the crystallite size, M_s the saturation magnetization, k_1 the magnetoctystalline anisotropy, T_c the Curie temperature, k the Boltzman constant and a the lattice constant. L_{ex} can be calculated as:

$$L_{ex} = \sqrt{\frac{A}{k_1}} \tag{5}$$

where A is the exchange stiffness constant. At the grain sizes above L_{ex} the grain boundaries result in the pinning of the domain walls. Increasing the volume fraction of grain boundaries through grain refinement impedes the domain wall movement, thereby increasing the coercivity [15,27]. When the grain size is smaller than the magnetic exchange length, domain wall effect diminishes and each grain behaves as a single domain. Based on the random anisotropy model, the coercivity can be expressed as [15,28]

$$H_c = \frac{p_c k_1^4 D^6}{\mu_0 M_s A^3} \tag{6}$$

where A is the exchange stiffness constant, p_c a constant of the order of unity and μ_0 the permeability of free space.

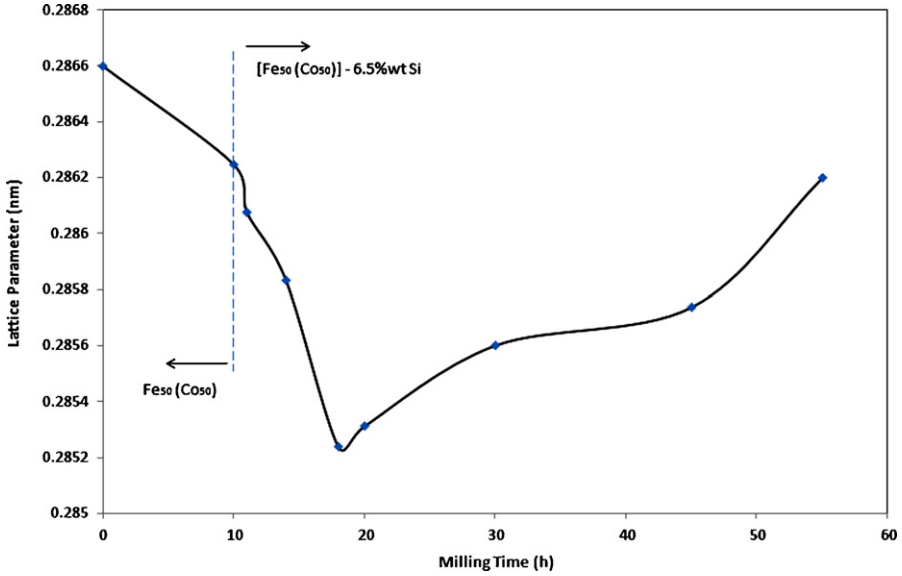

Fig. 7. Variations of lattice parameter with milling time.

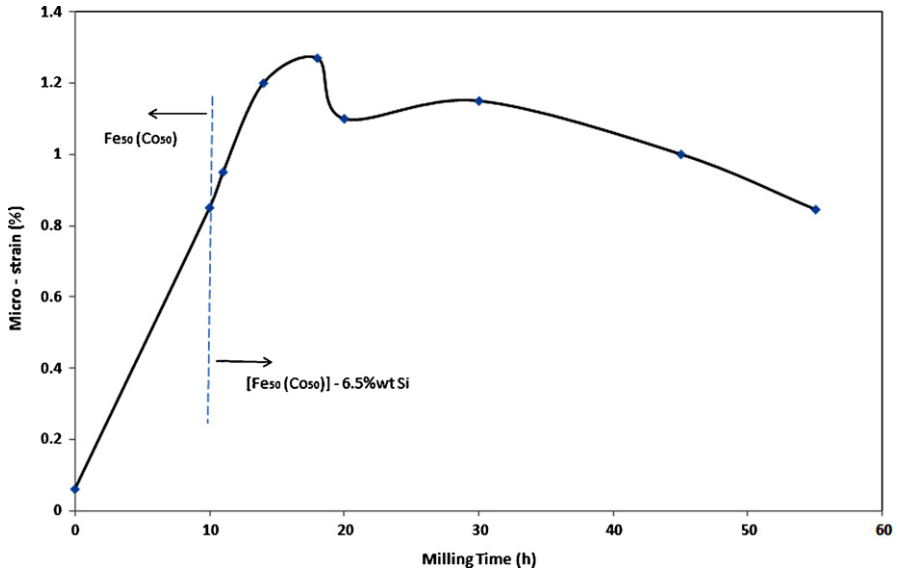

Fig. 8. Variations of internal micro-stress vs. milling time.

The unexpected increment of coercivity is due to the fact that in ferromagnetic materials, the permanent unpaired dipoles easily line up with the imposed magnetic field due to the exchange interaction or mutual reinforcement of the dipoles [4]. The exchange interaction then occurs over several grains forcing the magnetization vectors in each grain to be parallel to each other. This leads to better soft magnetic properties such as higher permeability and lower coercivity [29]. The degree of exchange interaction between the grains depends on the thickness and magnetic structure of the interface (grain boundary) [3]. Narrow grain boundary regions originate a large exchange interaction coupling between neighboring grains thus in the boundary region limiting two grains a structure of magnetic moments allowing a gradual transition between the local easy axes direction is formed [3]. But where the ferromagnetic grains are separated by nonmagnetic or less-magnetic grain boundaries thus the coupling between the ferromagnetic grains becomes less effective [26]. The coercivity is also determined by the magnitude of the exchange and dipolar magnetic interaction, which determine the degree of collectiveness of the reversal process [3].

In this work after adding Si and continuance of milling from 10 h up to 45 h (in fact total milling time is 20–55 h) the concentration of Si atoms in grain boundaries increases and since Si is a diamagnetic element, this leads to the decrease of the exchange interaction between grains and subsequently increasing the coercivity.

On the other hand, it has been suggested that the coercivity is strongly dependent on particle size. Generally, smaller particle size can result in higher coercivity [30]. Since the particle size also decreases with milling time at these stages, it can be expected that the coercivity also increases. In a soft magnetic random anisotropy system with high dislocation density (residual stress), the effective anisotropy constant is given by [27]:

$$K_{\text{eff}} \approx \frac{\sqrt{k_{\sigma,\text{ma}}^2 + \langle k_{\sigma,\text{mi}} \rangle^2 + \langle k_1 \rangle^2}}{\sqrt{d^3}} \tag{7}$$

where k_1 is the magnetocrystalline anisotropy of the material, $K_{\sigma,\text{ma}}$ and $K_{\sigma,\text{mi}}$ are averaged long-range and short-range magnetoelastic anisotropies, respectively and d is the average particle size.

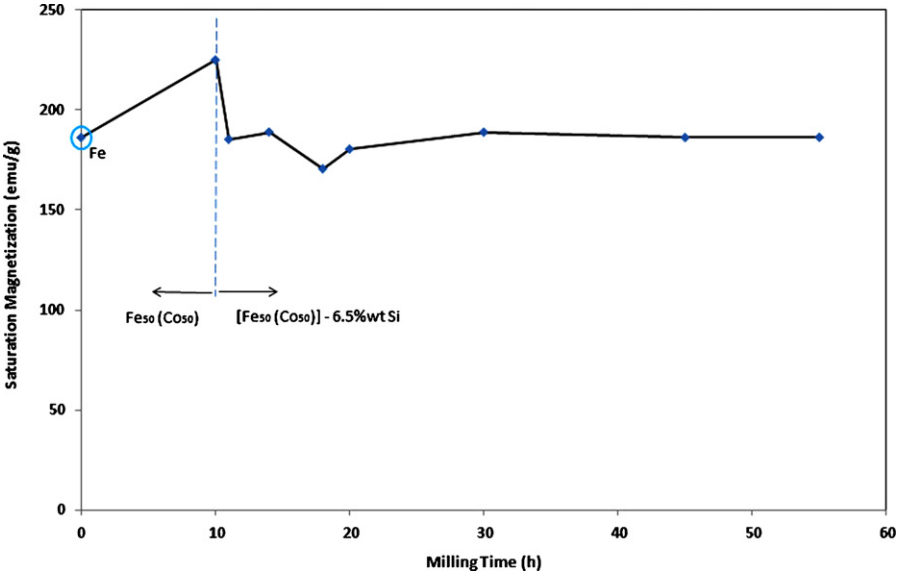

Fig. 9. Variations of saturation magnetization with milling time.

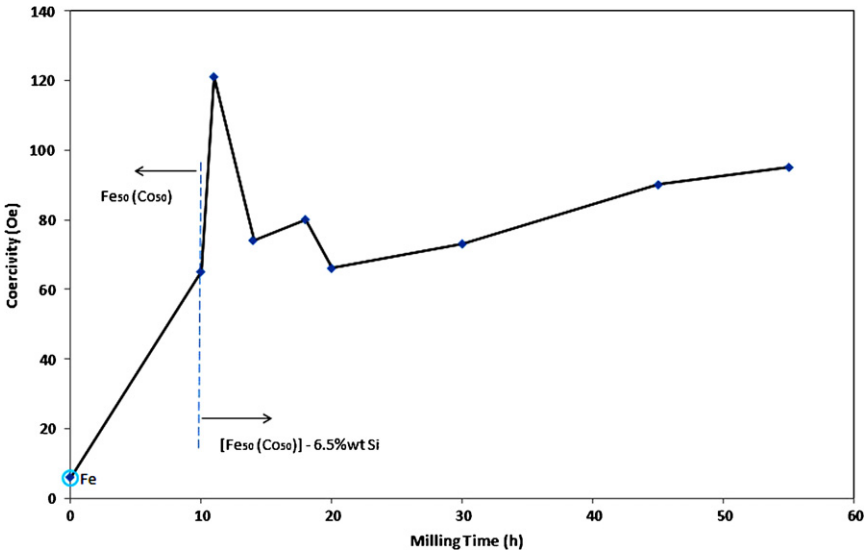

Fig. 10. Variations of coercivity with milling time.

This equation shows that with decreasing particle size, effective anisotropy constant increases and with increasing this, coercivity increases.

Obviously, the amount of the coercivity obtained in this work is extremely high. However, these high values of coercivity have been reported by other researchers [7]. Ding et al. [9] have proposed that high values of coercivity in nanostructured Fe–Si powders are due to strains developed during severe plastic deformation.

4. Conclusions

The following points can be drawn from the results of this work:

1. In the early stage of ball milling, the Fe(Co,Si) particle size has increased (due to cold welding), but further milling has caused a drastic reduction in particle size (cold welding dominated by fracturing) and prolonged milling has caused steady state (due to the equilibrium between the rate of cold welding and fracturing).
2. The minimum crystallite size achievable by milling process is more dependent on milling energy rather than on chemical composition powders.
3. The micro-strain will increase drastically due to the introduction of crystal defects induced by milling process, but migration of Si atoms from grains to grain boundaries will reduce the crystal distortion which leads to lower internal micro-strain.
4. Reduction of lattice parameter is due to the dissolution of solute atoms (Co and Si) which have different atomic size compared with solvent (Fe) atoms. With increasing the milling time, the solute atoms will leave the grains and this will lead to the increase of the lattice parameter. Another reason for the growth of lattice parameter is the higher volume fraction of grain boundaries which induced a negative pressure into the lattice.
5. Addition of Si, decreases M_s (since Si is a diamagnetic element). However the measured M_s for $[Fe_{50}(Co_{50})]$–6.5 wt% Si is reasonable in comparison with those of other Fe–Si systems.
6. Increment of coercivity at prolonged milling times could be due to segregation of Si atoms into the grain boundaries and decrement of the exchange interactions between the grains.

References

[1] H. Shokrollahi, K. Janghorban, Mater. Process. Technol. 189 (2007) 1–12.
[2] R. Koohkan, S. Sharafi, H. Shokrollahi, K. Janghorban, J. Magn. Magn. Mater. 320 (2008) 1089–1094.
[3] A. Hernando, J.M. González, J. Hyperfine Interact. 130 (2000) 221–240.
[4] D.R. Askeland, The Science and Engineering of Materials, third ed., PSW Publishing Company, Boston, 1994.
[5] H. Shokrollahi, J. Mater. Des. 30 (2009) 3374–3387.
[6] S.H. Kim, Y.J. Lee, B.H. Lee, K.H. Lee, K. Narasimhan, Y.D. Kim, J. Alloys Compd. 424 (2006) 204–208.
[7] S. Miraghaei, P. Abachi, H.R. Madaah-Hosseini, A. Bahrami, J. Mater. Process. Technol. 203 (2008) 554–560.
[8] M. Abdellaoui, T. Barradi, E. Gaffet, J. Alloys Compd. 198 (1993) 155–164.
[9] J. Ding, Y. Li, L.F. Chen, C.R. Deng, Y. Shi, Y.S. Chow, T.B. Gang, J. Alloys Compd. 314 (2001) 262–267.
[10] G. Tian, X. Bi, J. Alloys Compd. 502 (2010) 1–4.
[11] M.D. Chermahinia, H. Shokrollahib, J. Alloys Compd. 480 (2009) 161–166.
[12] Y. Liu, J. Zhang, L. Yu, G. Jia, C. Jing, S. Cao, J. Alloys Compd. 377 (2004) 202–206.
[13] T. Sourmail, J. Prog. Mater. Sci. 50 (2005) 816–880.
[14] M. Delshad Chermahini, S. Sharafi, H. Shokrollahi, M. Zandrahimi, J. Alloys Compd. 474 (2009) 18–22.
[15] M. Delshad Chermahini, S. Sharafi, H. Shokrollahi, M. Zandrahimi, A. Shafyei, J. Alloys Compd. 484 (2009) 54–58.
[16] B.H. Lee, B.S. Ahn, D.G. Kim, S.T. Oh, H. Jeon, J. Ahn, Y.D. Kim, J. Mater. Lett. 57 (2003) 1103–1107.
[17] B. Zuo, T. Sritharan, J. Acta Mater. 53 (2005) 1233–1239.
[18] Y.D. Kim, J.Y. Chung, J. Kim, H. Jeon, J. Mater. Sci. Eng. A 291 (2000) 17–21.
[19] C. Suryanarayana, Prog. Mater. Sci. 46 (2001) 1–184.
[20] H. Moumeni, A. Nemamcha, S. Alleg, J.M. Grenèche, J. Mater. Chem. Phys. 122 (2010) 439–443.
[21] M.D. Chermahini, M. Zandrahimi, H. Shokrollahi, S. Sharafi, J. Alloys Compd. 477 (2009) 45–50.
[22] B. Cantor, Novel Nanocrystalline Alloys and Magnetic Nanomaterials, IOP, Oxford, UK, 2005.
[23] Z. Bensebaa, B. Bouzabata, A. Otmani, J. Alloys Compd. 469 (2008) 24–27.
[24] M. Zandrahimi, M. Delshad Chermahini, M.H. Mirbeik, J. Magn. Magn. Mater. 323 (2011) 669–674.
[25] N.E. Fenineche, R. Hamzaoui, O. El Kedim, J. Mater. Lett. 57 (2003) 4165–4169.
[26] S. Allega, S. Azzazaa, R. Bensalema, J.J. Sunolb, S. Khenec, G. Fillion, J. Alloys Compd. 482 (2009) 86–89.
[27] M.P.C. Kalita, A. Perumal, A. Srinivasan, J. Magn. Magn. Mater. 320 (2008) 2780–2783.
[28] A.H. Taghvaei, A. Ebrahimi, M. Ghaffari, K. Janghorban, J. Magn. Magn. Mater. 323 (2011) 150–156.
[29] B. Zuo, N. Saraswati, T. Sritharan, H.H. Hng, J. Mater. Sci. Eng. A 371 (2004) 210–216.
[30] J. Ding, Y. Shi, L.F. Chen, C.R. Deng, S.H. Fuh, Y. Li, J. Magn. Magn. Mater. 247 (2002) 249–256.